State-specific morphological deformations of the lipid bilayer explain mechanosensitive gating of MscS ion channels

Yein Christina Park[1], Bharat Reddy[2], Navid Bavi[2],

Eduardo Perozo[2]* and José D. Faraldo-Gómez[1]*

[1]Theoretical Molecular Biophysics Laboratory
National Heart, Lung and Blood Institute
National Institutes of Health, Bethesda, MD

[2]Department of Biochemistry and Molecular Biology
University of Chicago, Chicago, IL

*Correspondence should be addressed to:

eduardo.perozo@uchicago.edu
jose.faraldo@nih.gov

July 1st, 2022

ABSTRACT

The so-called force-from-lipids hypothesis of cellular mechanosensation posits that ion channel gating directly responds to changes in the physical state of the membrane induced for example by lateral tension. Here, we investigate the molecular basis for this transduction mechanism by studying the mechanosensitive ion channel MscS from *Escherichia coli* and its eukaryotic homolog, MSL1 from *Arabidopsis thaliana.* First, we use single-particle cryo-EM to determine the structure of a novel open conformation of wild-type MscS, stabilize in thinned lipid nanodisc. Compared with the closed state, the structure shows a reconfiguration of helices TM1, TM2 and TM3a, resulting in widening of the central pore. Based on these structures, we examined how the morphology of the lipid bilayer is altered upon gating, using molecular dynamics simulations. The simulations reveal that, in the absence of extrinsic forces, closed-state MscS causes drastic protrusions in the inner leaflet of the lipid bilayer. These deformations develop to provide adequate solvation to hydrophobic features of the protein surface, and clearly reflect a high energy conformation for the membrane. Strikingly, the protrusions are largely eradicated upon channel opening. An analogous computational study of open and closed states of MSL1 recapitulates these findings. The gating equilibrium of MscS channels thus appears to be dictated by two opposing conformational preferences, namely those of the lipid membrane and of the protein structure. We theorize that membrane tension controls this balance because it increases the energetic cost of the membrane deformations that specifically stabilize the closed channel, shifting the gating equilibrium towards the conductive form.

INTRODUCTION

Sensory perception is a defining characteristic of life. In a constantly changing environment, cells must be able to detect a variety of stimuli, ranging from electric fields and chemical gradients to temperature and pressure. To respond to these inputs, cells have evolved a wide array of specialized membrane proteins; among these are mechanosensitive ion channels, which are activated by mechanical forces exerted on the cell. Broadly speaking, mechanosensitive channels fall in two classes: those that respond to changes in membrane tension, and those that transduce other structural perturbations. Examples in the latter class include NOMPC channels, which open upon compression of their molecular structure against the microtubule network to which they are tethered [1]. PIEZO, by contrast, belongs to the class of channels directly sensitive to lateral membrane tension [2-4], through a mechanism that has been referred to involving a "force-from-lipids" [5, 6]; this class also includes MscL and MscS, two extensively characterized channels whose physiological role is to relieve osmotic stresses to as to prevent cell rupture [2-4, 7, 8].

The force-from-lipids hypothesis, while firmly established by functional assays, remains to be rationalized at the molecular and physical levels. One challenge is that mechanosensitive channel families strongly diverge structurally [2, 3, 7, 9, 10], seemingly reflecting the cell's ability to detect a variety of mechanical stimuli with different degrees of sensitivity [4]. It is thus conceivable that evolution has led to different realizations of the force-from-lipids principle too. Even so, it is worth noting that channels within the same family, and hence a shared molecular mechanism, operate in vastly different membrane contexts. MscS channels, for example, have been identified in bacteria, archaea, fungi, and plants [9, 11]. This ubiquity across kingdoms of life raises intriguing questions: what single mechanism of tension sensing could accommodate these very different lipid environments? And might that mechanism be transferable not only across species but also among entirely different families of mechanosensitive channels?

Here, we focus on two channels of the MscS family that have been structurally characterized in multiple functional states, namely the *Escherichia coli* mechanosensitive channel of small conductance, EcMscS (or MscS) and its homolog in *Arabidopsis thaliana*, AtMSL1 (or MSL1). MscS resides in the inner membrane of *E. coli* and opens under moderate membrane tensions (5.5 mN/m in liposome patches [7]) to permit the flow of ions and water [3]. All available MscS structures, obtained through either X-ray crystallography or cryo-EM [12-17], show that this channel is a homoheptamer, featuring a transmembrane domain and a cytosolic domain. In the

transmembrane domain, so-called helix TM3a from each protomer forms a central pore that serves as the ion conduction pathway, flanked by helices TM1 and TM2, which face the lipid bilayer. It is through changes in the ternary and quaternary structure of this domain that MscS opens and closes. Specifically, in each protomer the TM1-TM2 hairpin changes tilt relative to both TM3a and to the membrane plane, and in turn this change results in widening or narrowing of the central pore. The magnitude of these changes has not been entirely clear, though, as the conducting state of the channel has been more difficult to capture than the closed form. Putatively open states have thus far resulted from either stabilizing point mutations [13, 14, 16] or solubilization in extremely thin lipid bilayers [16] or specific detergents [15], leading to slight differences in the structure. In contrast to the transmembrane domain, the cytosolic domain and the elements that connect it with the pore (that is, TM3b) are largely unchanged during channel gating; this domain thus appears to function as a sieve to prevent leakage of metabolically important small molecules [7], while enhancing the stability of the oligomeric complex, whether in the open or closed state.

Structures of closed and open states of MSL1 show a great degree of similarity with MscS, both in their overall architecture as well as in the conformational changes involved in gating. MSL1 is localized in the inner membranes of the *A. thaliana* mitochondria, where it is believed to contribute to dissipating the membrane potential under certain physiological conditions [18]. When expressed in *E. coli*, MSL1 can protect the bacteria from hypo-osmotic stress, although much less effectively than MscS [19]. MSL1 is predicted to feature two additional N-terminal helices, for a total of five (TM(-1) to TM3, following MscS nomenclature), but these additional elements have not been resolved in existing structures [18, 19]. Its pore-forming unit is however equivalent to that of MscS.

While the structural mechanism associated with MscS channel gating appears to be largely delineated, how this mechanism is influenced by lateral tension has been an elusive question. Tension is known to alter several bulk properties of the lipid bilayer, such as thickness, curvature, and lateral pressure [8, 20]; however, it is important to recognize that any model predicated on substantial modifications in the bulk properties of the membrane presupposes that these changes are not deleterious to other proteins embedded in or associated with the lipid bilayer. Moreover, it is unclear whether the moderate tensions that activate MscS can indeed effect changes in these properties of sufficient magnitude to explain the sensitivity of these channels, or how these putative changes would specifically favor the open state. Indeed, when attempting to formulate a theory of

mechanosensation, the challenge lies not only in identifying molecular features that are specific to the channel in question and that vary with its functional state; it is also crucial that these distinctive features be differentially influenced by tension in the open and closed states.

In this study we present structural and computational data that leads to a model of mechanosensation that satisfies these criteria. Specifically, we observe that the morphology of the lipid bilayer in the proximity to the protein is strongly deformed for the closed, but not the open state, and propose that tension shifts the gating equilibrium in favor of the open state because it increases the energetic cost of these membrane deformations. This model does not presuppose the existence of long-lasting protein-lipid interactions that are somehow weakened under tension. Instead, our view recognizes that the lipid bilayer is a structure with defined morphological energetics, and at the same time, a highly concentrated liquid solvent in constant motion at the molecular level.

RESULTS

Structure of an open conformation of MscS in a PC14:1 lipid bilayer

To determine an open-state structure of wild-type (wt) MscS in conditions that resemble a lipid membrane, we purified the channel and reconstituted it into nanodics consisting of myristoyl-phosphatidylcholine PC14:1 lipids and MSP1 E3D1 scaffold proteins, which we then imaged using single-particle cryo-electron microscopy (cryo-EM). (Alternative preparations of the wild-type channel using PC14:0 lipids or of the A106V mutant in dioleoyl-phosphatidylcholine PC18:1 nanodics failed to reveal an open state, and instead resulted in a conformation indistinguishable from that of the known closed state, not shown.) The resulting cryo-EM structure of wt-MscS in PC14:1 is shown in **Figure 1A**. The resolution of the structure is approximately 3.1 Å; density signals can be discerned and traced for most of the polypeptide chain, except for residues 1-15 at the N-terminus, for which only the Cα trace might be approximately inferred using molecular dynamic flexible fitting. The structure recapitulates known features of the MscS heptameric architecture; that is, a large intracellular domain, which features numerous contacts among protomers and appears to facilitate oligomerization, and a much more loosely packed transmembrane domain, which responds to the physical state of the membrane, and which consists of helices TM1, TM2 and TM3 in each protomer. As observed in previous structures of MscS (REFS), TM3 is not a continuous helix but breaks into two distinct segments, approximately halfway. The N-terminal fragment, TM3a, flanks much of transmembrane portion of the ion permeation pathway (**Figure 1B**), while TM1 and TM2 are positioned peripherally towards the lipid bilayer. The C-terminal fragment of TM3, TM3b, serves as the linker to the intracellular domain. It is at the junction between TM3a and TM3b where the ion permeation pathway is narrowest in this structure; however, at this point the pore diameter is ~13 Å, which is sufficient to permit flow of hydrated cations. The cryo-EM map reveals no evidence of any obstructions (such as lipids) of this seemingly open pore.

Figure 2A compares the structures of the putatively open state of wt-MscS obtained in PC14:1 lipid nanodiscs and that of the closed state we previously determined in PC18:1 [17]. No significant differences exist in the intracellular domain or its arrangement relative to the TM3b linker; the internal structure of the TM1-TM2 hairpin is also largely invariant. By contrast, there is a drastic reorientation of the TM1-TM2 hairpin, relative to TM3a as well as the membrane plane.

TM1 specifically tilts by 43º towards the plane of the bilayer upon channel opening, and TM2 tilts alongside by 40º. This reorientation of the TM1-TM2 hairpin permits TM3a to alter its angle relative to TM3b and retract away from pore axis, thereby widening the permeation pathway. This drastic change in the TM1-TM2 hairpin, which is symmetrically replicated in all protomers, also translates into a marked reduction in the width of the transmembrane span of the channel. This reduction is likely one of the factors that explain why the open conformation is favored upon reconstitution in PC14:1 nanodiscs, while PC18:1 nanodics stabilize instead the closed state [17]; indeed, as shown in **Figure 2B**, nanodisc morphologies are clearly discernable in the cryo-EM maps and appear to adequately match the different widths of the protein transmembrane span.

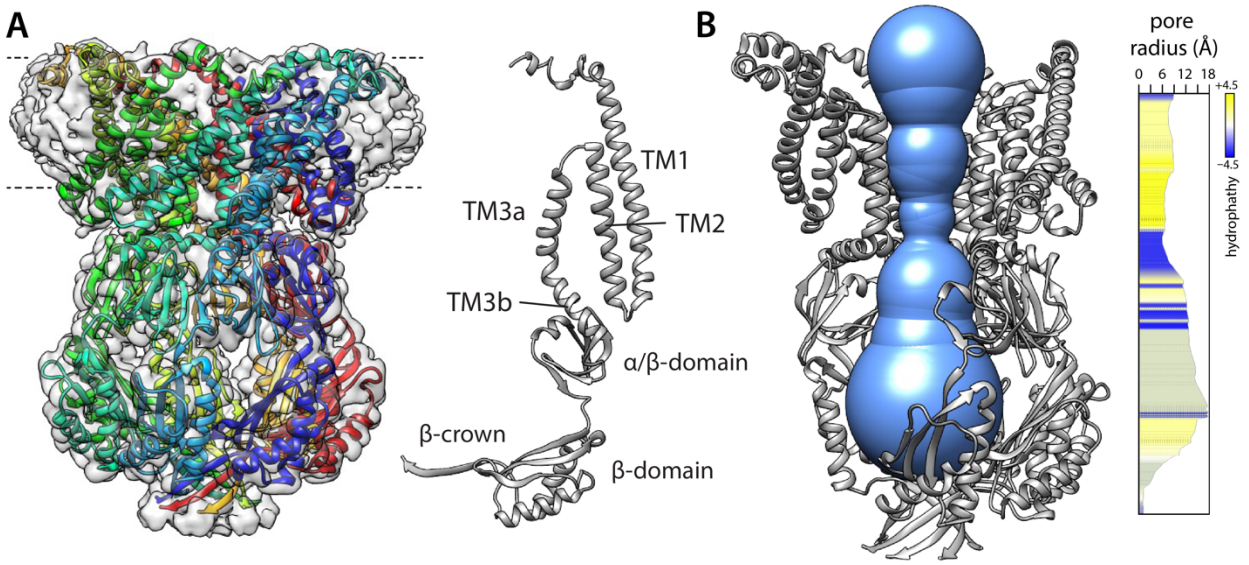

Figure 1. Structure of a putatively open conformation of wild-type MscS in a lipid nanodisc. (**A**) Left, structure of the MscS heptamer (in cartoon representation) fitted on the 3.1-Å resolution cryo-EM map (transparent surface). Each protomer is shown in a different color. The approximate location of the lipid bilayer is indicated with dashed lines. Right, cartoon representation of an individual protomer. (**B**) Cutaway of the structure (minus 2 protomers) showing the shape of the ion permeation pathway as determined by MOLEonline [21]. The rightmost plot quantifies the radius along the central symmetry axis as well as the hydrophobicity of the pore amino-acid make up.

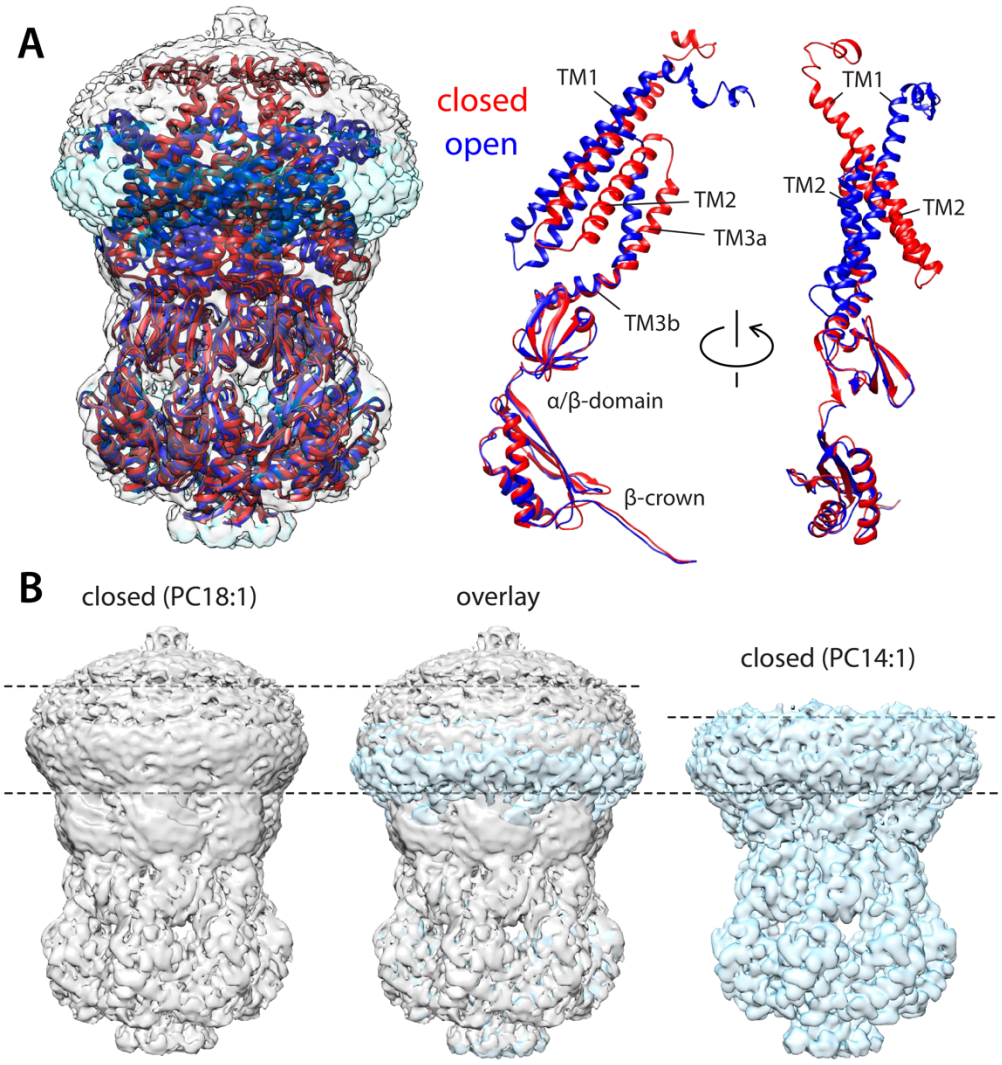

Figure 2. Comparison of closed and open structures of MscS in lipid nanodiscs. (**A**) Left, the open structure of MscS in PC14:1 lipid nanodiscs (blue cartoons) is superposed onto that of the closed state (red state), previously determined in PC18:1 nanodiscs (PDBID 6PWN, and EMD-20508). The corresponding cryo-EM density maps (transparent cyan and gray surfaces, respectively) are shown as well. Right, conformational change in each of the protomers. (**B**) Side-by-side comparison of the cryo-EM density maps obtained in PC18:1 (gray) and PC14:1 (cyan), alongside their overlap. The comparison clearly highlights the reduction in the width of the transmembrane span of the channel upon opening, and how this changed is well matched by the thickness of the corresponding lipid nanodiscs (approximately from 38 to 23 Å).

Figure 3 compares the structure of wt-MscS described above with two others reported previously and proposed to capture open or partially open conformations of the channel: that of a mutant

(A106V), crystallized in detergent micelles and resolved through X-ray diffraction [13]; and that of wt-MscS reconstituted in PC10:0 lipid nanodiscs, imaged with single-particle cryo-EM [16]. This comparison makes it clear that the extent of the conformational changes observed in our structure is significantly amplified in those existing structures. For example, TM1 tilts up to 54-55º, and TM2 tilts by 45-47º (**Figure 3A**). However, these differences have a minor impact on the dimensions of the pore, whose diameter is, at most, only 2 Å wider (**Figure 3B**). Admittedly, none of the three structures captures the channel embedded in a native membrane; arguably, though, a PC14:1 nanodisc is a more realistic mimic than a detergent micelle or a PC10:0 nanodisc. Since the conformational changes observed in the PC14:1 structure appear sufficient to open up the ion permeation pathway, we posit that the structure of wt-MscS reported here is, at minimum, similarly likely to represent the conductive form of the channel in physiological conditions.

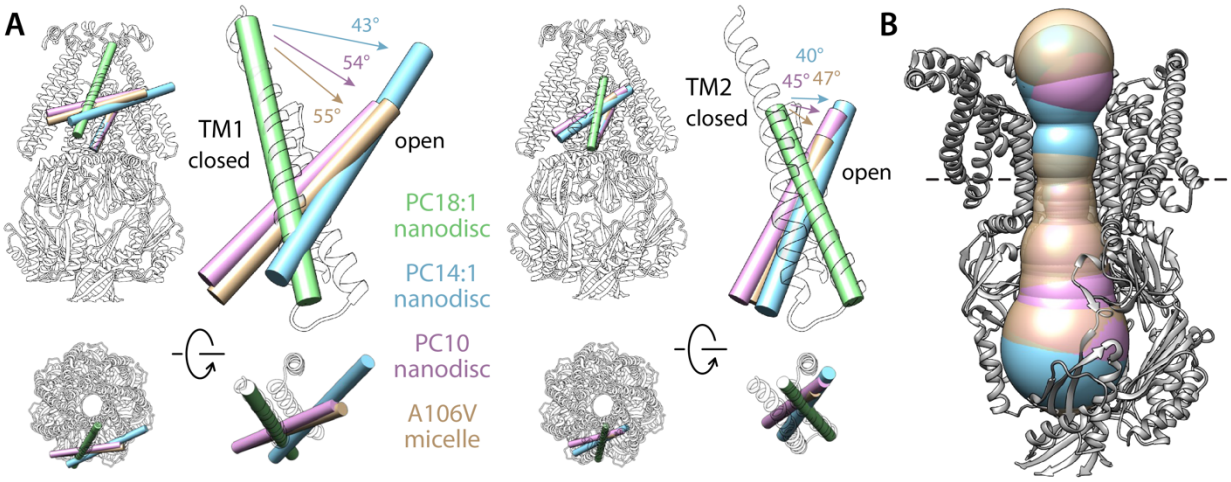

Figure 3. Comparison of alternate conformation of open MscS obtained in different experimental conditions. (**A**) Overlay comparing helices TM1 and TM2 in the closed state (green tube and white cartoons,) and in the putatively open states obtained in PC14:1 nanodiscs (this work, cyan), in PC10 nanodiscs (PDB 6VYL, pink) and in detergent micelles (PDBID 2VV5, orange). Note the structures in lipid nanodisc were determined with single-particle cryo-EM for the wild-type protein, while the A106V structure in detergent was determined with X-ray crystallography. All structures are superimposed based on TM3. (**B**) Comparison of the dimensions of the permeation pore in the three structures of the putatively open state. The black dashed line indicates the position of L105, which is approximately where the pore is narrowest; the radius here is 6.3 Å for the PC14:1 structure, 6.7 Å for the PC10 structure, and 7.5 Å for the mutant in detergent.

Table 1. Molecular simulation systems evaluated in this study of McsS and MSL1 mechanosensation.

	MscS coarse grained[a]							**MscS all atom**[b]		**MSL1 coarse grained**[a]	
	Closed WT POPC	Closed WT POPC	Closed WT DMPC	Closed WT PC:PG	Open WT POPC	Open A106V POPC	Open D67R1 POPC	Closed WT POPC	Closed WT DMPC	Closed WT POPC	Open WT POPC
Protein	1	1	1	1	1	1	1	1	1	1	1
POPC	2057	755	0	1651	686	737	740	755	0	2001	1916
POPG	0	0	0	407	0	0	0	0	0	0	0
DMPC	0	0	768	0	0	0	0	0	768	0	0
Na^+	855	328	340	1265	328	328	328	314	326	855	855
Cl^-	862	335	347	865	335	356	349	335	347	890	883
Water[b]	75938	28123	29000	75501	28200	28372	28299	115170	118774	76076	76549
System size (nm)	26.5 × 26.5 × 18.7	16.9 × 16.9 × 17.9	16.3 × 16.3 × 19.1	26.3 × 26.3 × 19.0	16.9 × 16.9 × 17.9	16.9 × 16.9 × 17.9	16.9 × 16.9 × 17.9	15.9 × 15.9 × 19.9	15.4 × 15.4 × 21.1	26.5 × 26.5 × 18.7	26.5 × 26.5 × 18.7
Time (μs)	20	20	20	20	20	20	20	10	10	80	20

[(a)] MARTINI 2.2 forcefield. [(b)] CHARMM36m forcefield. [(c)] One CG water particle is equivalent to four AA water molecules.

Closed-state MscS induces drastic deformations of the lipid bilayer

To begin to investigate how the physical state of the lipid bilayer might influence the conformational equilibrium between conductive and non-conductive forms of McsS, we first examined the membrane morphology associated with the closed state of the channel, using the structure we previously resolved in PC18:1 lipid nanodiscs [17]. To that end, we carried out a series of molecular dynamics (MD) simulations, both based on coarse-grained (CG) and all-atom (AA) representations, evaluating multiple lipid bilayer compositions and membrane dimensions (**Table 1**). All CG trajectories lasted for 20 μs each and were initiated with a flat membrane; simulations were calculated independently of any experiments, and no prior assumptions were made in regard to the configuration of the protein-lipid interface (see Methods for further details). The AA trajectories were initiated in a representative configuration of a CG trajectory obtained under the same condition, and lasted 10 μs each. Invariably, these simulations showed that stabilization of the closed conformation of MscS demands drastic deformations in the morphology of the lipid bilayer, and in particular the inner leaflet. **Figure 4** depicts these deformations using 3D density maps derived from the simulated MD trajectories, for several of the different conditions explored. These density maps clearly reveal extensive protrusions in the inner leaflet of the membrane, which develop to provide adequate solvation to exposed hydrophobic surface in the protein in this particular state. These hydrophobic surfaces line crevices formed between the TM1-

TM2 hairpin and TM3a-TM3b, well outside what might be predicted as the transmembrane span of the channel; adequate lipid solvation of these cavities thus requires dramatic morphological changes in the bilayer. Logically, we detect seven nearly identical protrusions, matching the symmetry of the channel structure.

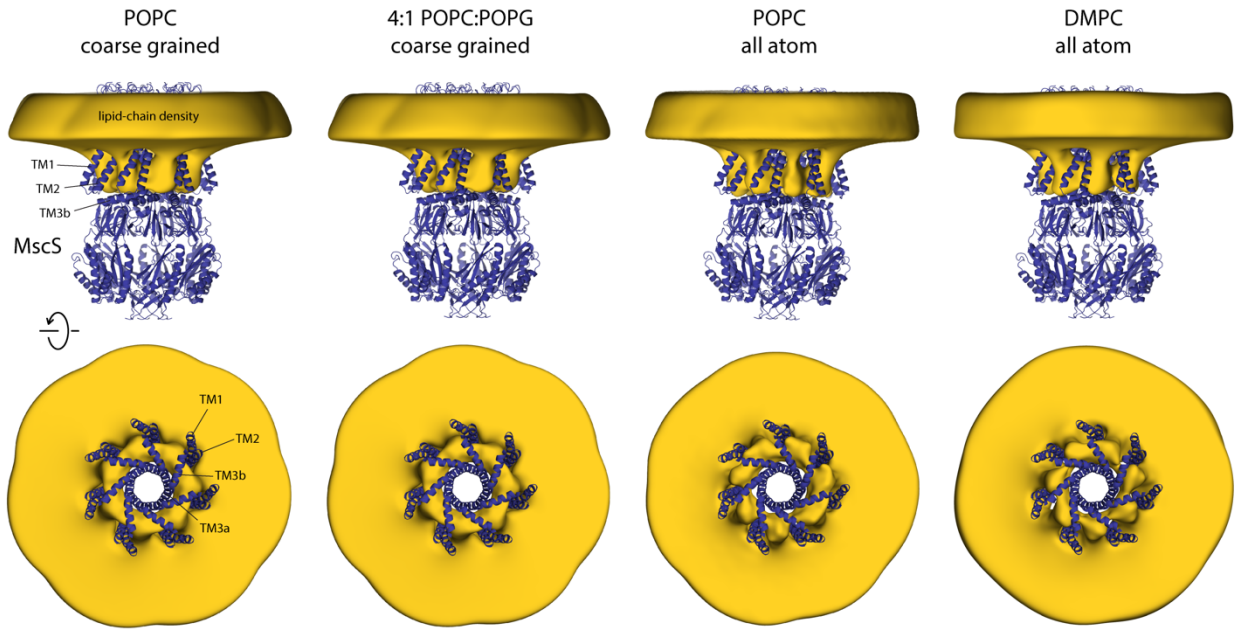

Figure 4. Closed-state MscS channel induces drastic perturbations of the lipid bilayer. The figure summarizes the results from multiple simulations of the closed structure of MscS in different membrane compositions and using different forcefield representations (Table 1). The cryo-EM structure of MscS (blue cartoons) is overlaid with calculated 3D density distributions mapping the morphology of the alkyl chain double layer in each of the MD trajectories (gold volume), up to 50 Å from the protein surface. Protein and density maps are viewed along the membrane plane (top row) and along the pore axis, from the cytosolic side (bottom row); the latter includes only the transmembrane domain of the channel, for clarity. The calculated density maps derive from 20 μs of trajectory data for each of the coarse-grained systems and 8 μs of trajectory data for the all-atom systems.

To more precisely discern the structure of these perturbations, we analyzed the average molecular configuration of the lipids found in these regions as well as elsewhere in the bilayer. As shown in **Figure 5**, it is striking that to form these protrusions the headgroup layer of the inner leaflet must not only project away from the membrane center but also bend sharply, thus permitting the underlying acyl chains to become strongly tilted, by as much as 60 degrees relative to the membrane perpendicular (**Supplementary Figure 1**). Importantly, examination of the lipid

translational dynamics makes it clear that the molecules in these protrusions are in constant exchange with the rest of the bilayer (**Figure 6**). As expected, the turnover of the lipids found in the protrusions is slower than elsewhere in the bilayer, but only by an order of magnitude. This observation is comparable for the CG and AA systems; naturally, lipid diffusion is artificially accelerated in the CG representation, but it seems fair to conclude that the lipid content of the inner leaflet protrusions would be renewed multiple times within tens of microseconds. Thus, in the context of the membrane, it seems hardly accurate to characterize these molecules as 'bound', as one would a conventional agonist or antagonist of a ligand-gated channel, for example. Instead, what we observe in these simulations is a reorganization of the structure and dynamics of the lipid solvent to adequately solvate the topography and amino-acid make-up of the protein surface in this particular state.

Finally, it is worth noting that the channel structure also bends the outer leaflet of the membrane, although to a much smaller degree (**Figures 4, 5**). The most significant perturbation in the outer leaflet is the sequestration of seven lipids (one per protomer), each of which fills the space in between adjacent TM1 helices; the polar headgroups of these lipids project towards the aqueous interior of the pore and interact with R88, riding over the short linker that connects TM2 and TM3 in each protomer. These molecules correspond exactly to density features in our cryo-EM map of the closed state [17], as well others reported subsequently [16], which we referred to as "hook lipids". Our simulations show that these lipids molecules are associated with the outer leaflet of the membrane, not the inner leaflet as previously theorized [16].

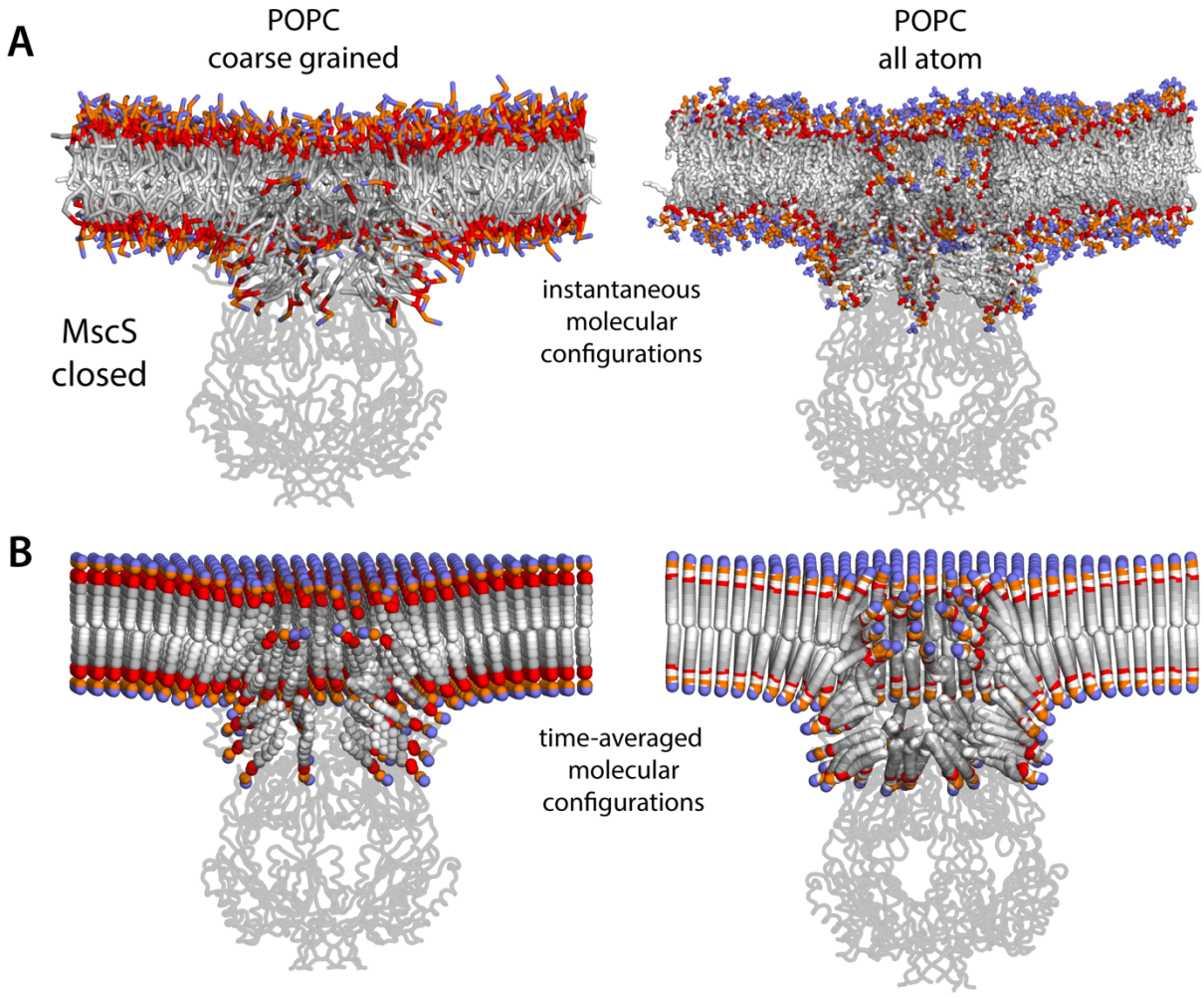

Figure 5. Molecular structure of the membrane perturbations induced by MscS channel in the closed state. (**A**) Instantaneous configurations of the lipid bilayer in single snapshots of two of the MD trajectories calculated for closed-state MscS in POPC, shown in cross section to reveal the structure of the perturbations induced by the protein. Choline groups are shown in purple, phosphate in orange, ester linkages in red and alkyl chains in shades of gray. The channel structure is overlaid, shown in cartoons. (**B**) Time-averages of the instantaneous lipid configurations observed in the same two trajectories, mapped across the membrane plane. Averages are calculated for each lipid atom and shown as spheres, colored as in panel (A). Owing to the configurational and rotational dynamics of lipids the resulting averages are non-physical structures, but they nevertheless capture the position and orientation adopted by lipid molecules in different regions the membrane. The average configuration of the channel backbone is also shown, overlaid. Protein and lipid averages derive from 20 μs of trajectory data for the coarse-grained system and 8 μs of trajectory data for the all-atom system. The figures in panel A show snapshots at $t \approx 7$ μs of the coarse-grained simulation and at $t \approx 5$ μs of the all-atom simulation.

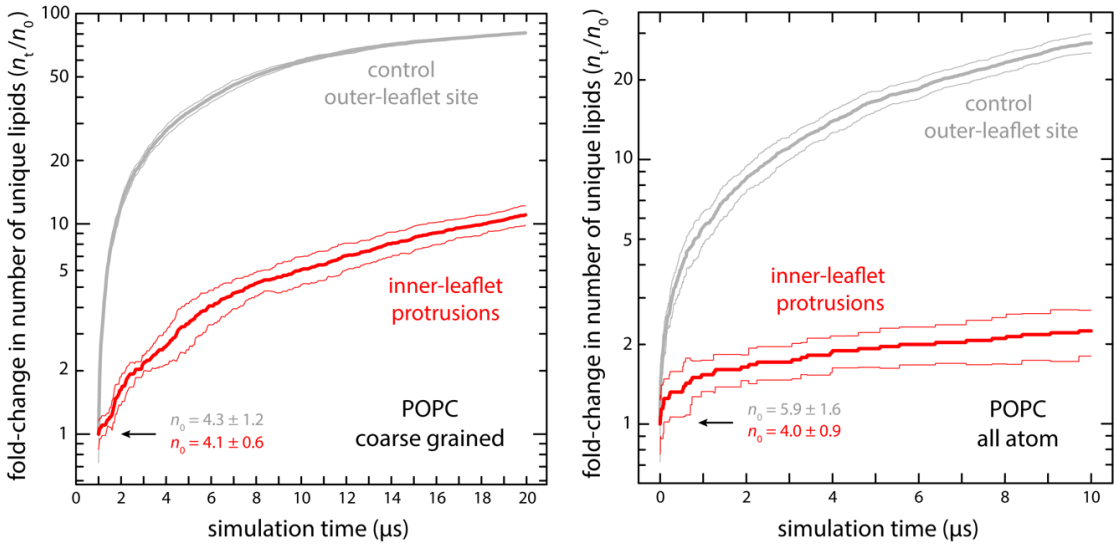

Figure 6. Lipids in inner-leaflet protrusions exchange with lipids in the bulk membrane. Time-course of the number of lipid molecules that are newly found within the inner-leaflet protrusions during the simulations of closed-state MscS in POPC using either a coarse-grained (left) or all-atom (right) representation (thick red lines). To monitor the exchange between bulk and protrusion lipids, we searched for lipid molecules within 20 Å of residue Ile150 at each simulation timepoint and identified those newly found; the cumulative number of these lipids, n_t, divided by the initial number of lipids in the protrusions, n_0, yields the fold-change factor shown in the plots. Data is averaged across the seven monomers; the standard deviation at each time point is indicated (thin red lines). For comparison, we carried out the same analysis for a control site on the protein surface exposed to the outer leaflet of the membrane (Gln21) (gray lines). The maximum possible values for the fold-change, based on the values of n_0 and of the total number of lipids in each leaflet, are as follows: 88.1 (CG, inner-leaflet protrusions); 91.0 (CG, control); 91.3 (AA, inner-leaflet protrusions); 66.9 (AA, control).

MscS opening eliminates deformations in the lipid bilayer

To shift the gating equilibrium of an ion channel, a given stimulus such as membrane tension must have a differential effect on the open and closed states. Following this reasoning, we next examined the morphology of the lipid bilayer that corresponds to the open state of MscS, using simulations of the new structure reported here. The central observation from this analysis is, strikingly, the near-complete eradication of the protrusions observed in the inner leaflet of the lipid bilayer for the closed state (**Figure 7**). This marked difference logically correlates with the structural changes observed in the channel; in the open state, the hydrophobic crevices formed between the TM1-TM2 hairpin and TM3a-TM3b are still filled with lipids, but the rotation of the TM1-TM2 hairpins aligns these crevices with the bulk membrane, and so these lipids do not protrude out (**Figure 7**),

nor do they become strongly tilted relative to the membrane perpendicular (**Supplementary Figure S1**). By contrast, the perturbation of the outer leaflet is largely identical to that observed for the closed state; the hook lipids sequestered in between adjacent TM1 helices, projecting into the pore over the TM2-TM3a linker, are also observed in the open state, and thus appear to be structural, rather than a differential characteristic of one state or the other. It is also interesting to note that despite the expansion of the pore, the total area of the protein-lipid interface as quantified by the number of chemical groups in the channel structure that are in direct or close-range contact with lipid molecules, is one 3% greater for the open state (**Supplementary Figure S2**). This seemingly counterintuitive result stems from the highly irregular morphology of the lipid bilayer in proximity to the close channel, and in our view underscores the inadequacy of geometric idealizations of the membrane, and of its interface with proteins.

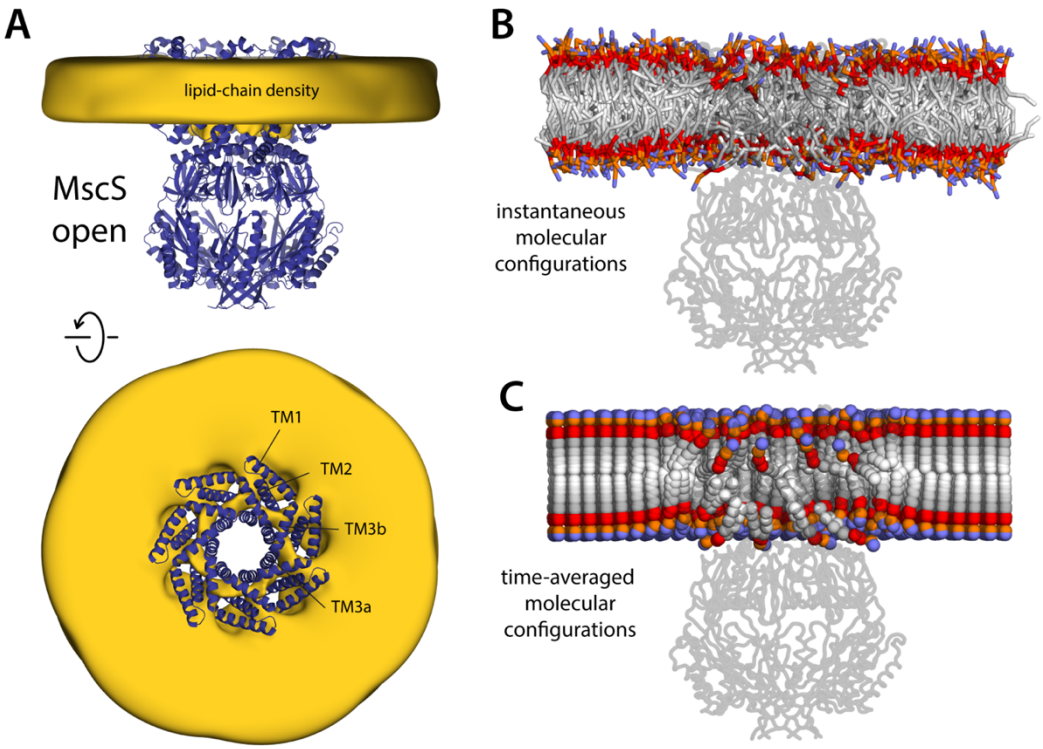

Figure 7. Membrane perturbations are largely eliminated upon MscS channel opening. The figure summarizes the results from a 20-μs simulation of open MscS in a POPC membrane, using a coarse-grained representation. (**A**) The cryo-EM structure of MscS in the open state (blue cartoons) is overlaid with a calculated 3D density distribution mapping the morphology of the alkyl chain double layer in the MD trajectory (gold volume), up to 50 Å from the protein surface. Protein and density maps are shown as in Fig. 3. (**B**) Instantaneous configuration of the lipid bilayer in a snapshot of the MD trajectory, shown in cross-section as Fig. 4A. (**C**) Time-averages of the instantaneous lipid configurations observed in the trajectory, mapped across the membrane plane and shown in cross-section. Averages were calculated and are represented as in Fig. 4B.

For completion, we also carried out simulations of two other structures of MscS widely regarded to capture the open state of MscS, namely those of mutants A106V [13] and D67R1 [14]. As discussed above, these structures were obtained in detergent and differ from our wild-type structure obtained in lipid nanodiscs in the degree of tilt of the TM2-TM3 unit, relative to the pore axis; another notable difference is that they do not resolve the first 24 N-terminal residues. These differences notwithstanding, the simulations carried out for these two structures reaffirm the results obtained for the open-state conformation reported here; that is, the hydrophobic crevices under TM1-TM2 units remain lipidated, but the strong protrusions of the inner leaflet seen for the closed state are largely eliminated (**Supplementary Figure S3**).

Mitochondrial MscS homolog also deforms the bilayer in the closed but not the open state

When considering the potential mechanistic significance of a given observation, it seems reasonable to evaluate its transferability across homologous systems in different species, or more broadly, across proteins featuring similar functional characteristics. This is not a trivial consideration in the case of mechanosensation, as the divergence between channels and species involves not only different proteins sequences and entirely different folds but also membranes of entirely different composition. For example, the cytoplasmic membrane of *E. coli* is ~75% PE, 20% PG and 5% CL [22], whereas inner mitochondrial membranes are 40% PC, 30% PE, 15% CL [23]. To begin to ascertain whether the observations described above for MscS translate to other homologs in this family, we examined the lipid bilayer morphologies that correspond to the open and closed states of MSL1, the MscS-like channel from *A. thaliana*. As shown in **Figure 8**, this analysis recapitulates the results obtained for the *E. coli* protein, despite the fact the MSL1 structures do not resolve the two N-terminal helices that precede TM1 in sequence. That is, the closed state of the channel induces drastic protrusions in the inner leaflet, which are largely eradicated in the open state. As in MscS, these protrusions stem from the need to provide adequate lipid solvation to hydrophobic crevices under the TM1-TM2 unit, which become strongly misaligned with the bilayer upon channel closing. The MSL1 simulations also show hook lipids interacting with the TM2-TM3 hairpin, but as with MscS, these lipids are observed in both states and thus do not appear to be a differentiating characteristic.

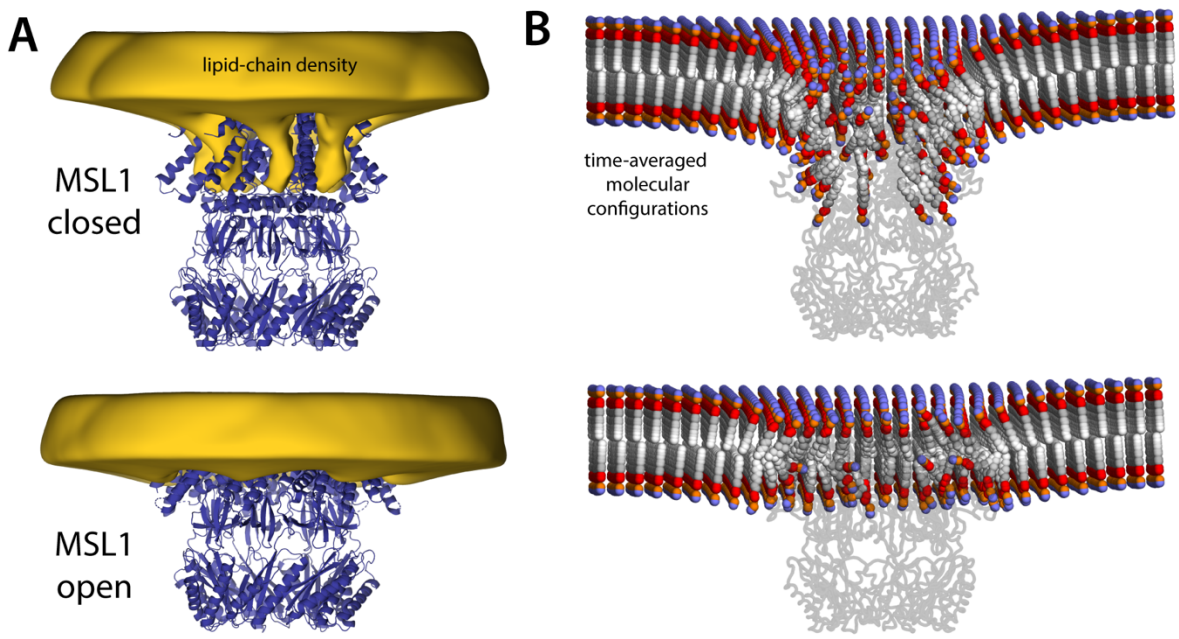

Figure 8. MSL1 gating causes morphological changes in membrane akin to those observed for MscS. The figure summarizes the results from a simulation of closed and open states of MSL1 in a POPC membrane, using a coarse-grained representation (Table 1). (**A**) The cryo-EM structures (blue cartoons) are overlaid with calculated 3D density distributions mapping the morphology of the alkyl chain double layer in each of the MD trajectories (gold volumes), up to 50 Å from the protein surface. Maps were calculated and are represented as in Fig. 3. (**B**) Time-averages of the instantaneous lipid configurations observed in each of the two MD trajectory, mapped across the membrane plane and shown in cross-section. Averages were calculated and are represented as in Fig. 4B. The datasets in panels (A) and (B) were symmetrized in accordance with the 7-fold internal symmetry of the channel.

DISCUSSION

It is increasingly recognized that lipid bilayers can deform to accommodate membrane protein structures [24]. It is worth keeping in mind, however, that all lipid bilayers, regardless of composition, resist deformations that are incongruent with their intrinsic curvature, and that this resistance increases when the membrane is stretched under tension. The apparent plasticity of the bilayer around membrane proteins thus reconciles two opposing free-energy contributions: the gains derived from adequate solvation of the hydrophilic and hydrophobic features of the protein surface, and the penalties incurred when the bilayer deviates from its preferred conformation. Lateral tension will alter this balance because it amplifies the cost of any morphological deformations, whether or not it affects the manner in which protein and lipids interact at close range. It follows that an ion channel that causes a strong perturbation in membrane shape in the closed state, but not in the conductive state, will respond to tension by increasing its open-state probability; that is, it will be mechanosensitive.

The computational and experimental data presented in this study for two MscS ion channels lend support to this molecular theory of mechanosensation, which departs from existing views of the force-from-lipids principle, as will be discussed below. We show evidence of drastic channel-induced perturbations in membrane morphology that are not only specific to the closed state of the channel but that also clearly deviate from the inherent conformational preference of the lipid bilayer. Logically, these perturbations stem from the structural features and chemical make-up of the protein surface; in particular, large hydrophobic cavities found between adjacent transmembrane elements, specifically the TM1-TM2 hairpin and TM3a. These cavities are naturally solvated by lipid molecules, in both open and closed states of the channel. But while adequate lipidation of the protein surface appears to be readily attained in the open state, the reconfiguration of the TM1-TM2 hairpin upon channel closure forces the lipid bilayer to deform. Specifically, the membrane develops a series of striking protrusions that project from surface of the inner leaflet by up to 30 Å, or about 75% of the total thickness of the bulk membrane (**Figure 4**). These protrusions are observed for two different MscS-like channels, one prokaryotic and the other eukaryotic, matching the heptameric symmetry of their structures; they are also observed for membranes of different size and lipid composition, whether examined with a coarse-grained (CG) or all-atom (AA) forcefield (**Figure 4, 8**). This internal consistency in the simulation data is reassuring; importantly, the protrusions we observe also explain why multiple structural studies

have detected density signals attributable to lipids under the TM1-TM2 hairpin, for both MscS [14-17] and MSL1 [18]. Nevertheless, we question the prevailing view that density signals of this kind are evidence of regulatory lipid binding sites; that is, we do not concur with the assumption that lipids regulate the gating equilibrium of MscS just like an agonist or antagonist would for a ligand-gated receptor-channel. The lipid bilayer, notwithstanding its morphological preferences, is after all a highly concentrated solvent in constant molecular motion. Thus, while snap-freezing conditions might produce strong density signals representing preferred lipid configurations (or averages thereof), in functional settings it seems highly probable that all lipid molecules solvating the protein are in constant exchange with the bulk membrane on a faster timescale than the gating equilibrium per se, including the lipids in the cavities under the TM1-TM2 hairpin. Indeed, our simulations provide evidence of this exchange, for both the CG and AA representations. The CG trajectories logically show a faster turnover as this representation artificially accelerates the self-diffusion of lipids (approximately 5-fold). But even after taking this acceleration in consideration, this lipid exchange is clearly rapid compared with the lifetime of the closed states of the channel, which is at minimum hundreds to thousands of microseconds [25]. Moreover, lipid densities in the cavities under the TM1-TM2 hairpin are not limited to the closed-state structures; analyses of open MSL1 [18] and open or "open-like" MscS (**Figures 1-2**) [14-16] have also reported the presence of phospholipids or hydrocarbon chains in these cavities. Just as we see in our simulations, however, in these open-like states of the channel these densities do not protrude out from the plane of the detergent micelle or the lipid nanodisc. Thus, the most defining characteristic of the functional state of MscS, aside from is structure, is the membrane protrusions that arise upon channel closing.

Our perspective is, therefore, that the gating mechanism of McsS reflects an equilibrium between alternate conformations of the channel as well as between alternate conformations of the lipid bilayer (**Figure 9**). More precisely, this equilibrium includes a non-conductive form that strongly deforms the membrane and a conductive state that does so to a much smaller degree. This differentiation is key to rationalize mechanosensation, as the intrinsic conformational energetics of the bilayer, which are just as relevant as those of the channel, are also directly modulated by tension. Specifically, we posit that applied tension shifts the gating equilibrium towards the open state because membrane stretching makes the protrusions characteristic of the closed channel more costly (**Figure 9**). We recognize that membrane shape is not the only difference between open and

closed states: as discussed, the protein structure changes noticeably, and consequently also its close-range interactions with lipids. Accordingly, one or the other state of the channel might be stabilized by extrinsic manipulations of the protein structure, such as mutations, or by specific solubilization conditions, as has been empirically observed [2, 12-16, 25-27]. It does not immediately follow, however, that differences in protein structure or its close-range interactions with lipids are sufficient to rationalize mechanosensitive gating, as it is unclear how lateral tension would influence these factors at the molecular level.

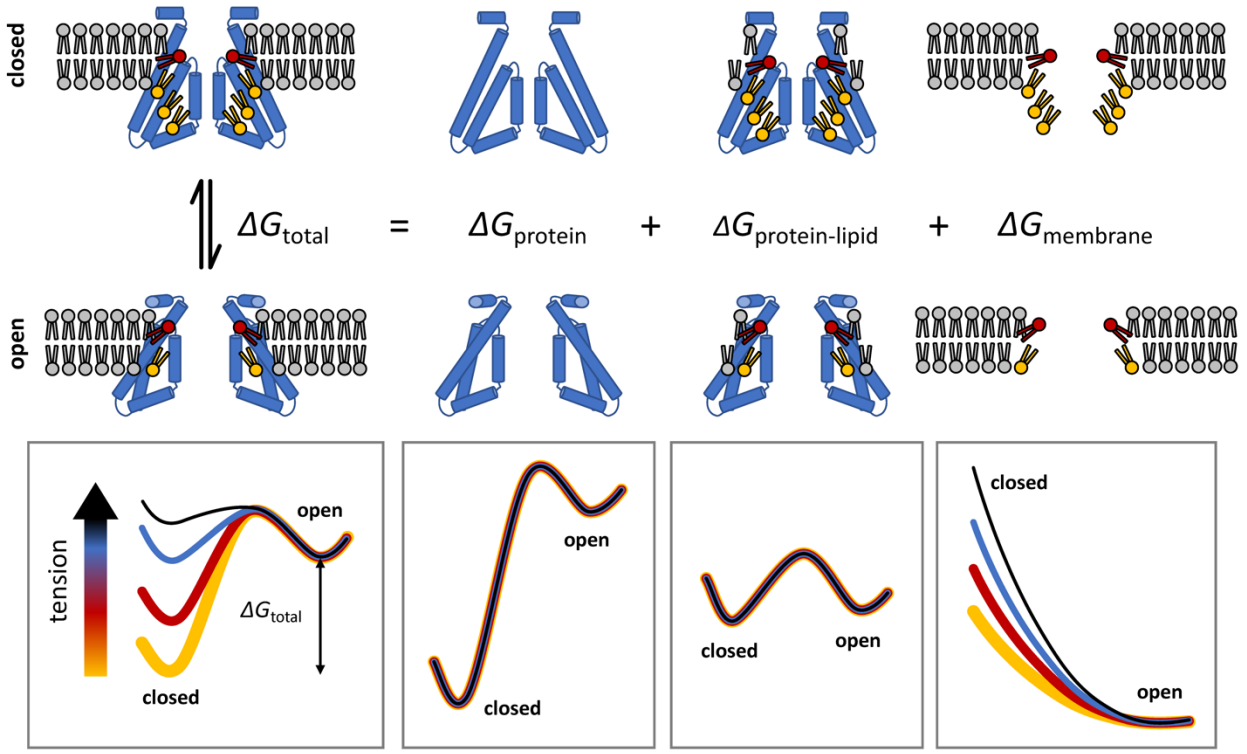

Figure 9. Conceptualization of the theory of mechanosensation proposed in this study. Lateral tension increases the open-state probability of MscS because membrane stretching increases the energetic cost of the deformations in the lipid bilayer that stabilize the closed conformation of the channel, which are largely eliminated when the structure opens. This rationalization of mechanosensitive gating does not presuppose that that closed state of the channel is structurally frustrated, but rather that it is highly stable, consistent with its greater compactness as well as with empirical observations. The proposed model also does assume that lateral tension must alter in any way the mode of interaction between the protein and its neighboring lipids, or that it causes putative lipid binding sites to be vacated or eliminated. Instead, this "membrane deformation model" recognizes that the inherent conformational preferences of the lipid bilayer contribute to dictate the overall energetics of the gating equilibrium, and that the cost of any deformation is invariably dependent on the degree of lateral stretching, regardless of lipid composition.

The theory of we propose, which could be referred to as "membrane deformation model", diverges substantially from other formulations of the force-from-lipids principle centered on the protein structure or the occupancy of putative lipid binding sites. For example, the "Jack-in-the-box" model is predicated on the assumption that the closed state of MscS is structurally frustrated, or strained, and proposes that membrane lipids exert a positive pressure that confines the protein to this unfavorable conformation [28]. In this model, membrane tension would shift the equilibrium towards the open state by decreasing this pressure, liberating the channel. While this mechanical analogy might seem intuitive, it is in our view hardly transferable to the molecular scale. Simulations show that lateral pressure profiles change modestly upon application of membrane tension [29], even for tensions 5 to 10 times greater than those sensed by MscS [30]. Moreover, as noted above the extent of the protein-lipid interface is comparable for open and closed states of MscS; if anything, this contact area is slightly expanded upon opening. Thus, irrespective of the degree to which increased tension reduces bilayer pressure on the protein surface, it seems unclear how this reduction would differentially favor channel opening. More importantly, perhaps, it is questionable that the closed structure is more strained or frustrated than that of the open state despite being patently more compact. To the contrary, a survey of existing structural studies of MscS, including those carried out in detergent micelles, show most conditions favor the closed state, especially for the wild-type channel [16, 17]. Indeed, we would argue that this inherent structural stability is expected, as it must counterbalance the cost of the membrane deformations characteristic of this conformation (**Figure 9**).

More recently, it has been proposed that delipidation of the grooves between the TM1-TM2 hairpin and TM3a explains MscS mechanosensitivity [15]. This "delipidation model" appears to be based upon the observation that the volume of these grooves, and therefore the number of lipids therein, diminishes in the open state relative to the closed state. While we concur with this structural observation, its relationship with mechanosensation is not self-evident in our view. As noted, the key question is not merely whether the lipidation of these grooves changes during gating, but whether tension has a differential effect on these lipidation numbers, when open and closed states are compared, in a manner that favors the former or disfavors the latter. Indeed, whether tension alone can alter the occupancy of these cavities, or any other putative lipid site, for any state of the channel, remains to be shown.

Admittedly, further work will also be required to further substantiate the theory of mechanosensation we propose. A particularly challenging but crucial task will be to formulate computational and experimental approaches to probe the conformational free-energy landscape of membranes, to clearly quantify the impact of variations in lateral tension and lipid composition, among other factors. From a computational perspective, we would argue it is imperative not to abandon molecular representations of the lipid bilayer and its interface with proteins, to be able to examine heterogeneous membranes and intricate morphologies with few a priori assumptions. Advanced MD simulation methods specifically designed to probe the conformational energetics of the membrane are therefore a promising route [31, 32]. In addition, as structural data becomes newly available for different functional states of other MscS channels, such as YbiO and YnaI [10], it will be of interest to examine whether they too induce state-specific deformations in membrane morphology. Similarly, it will be interesting to establish whether the conclusions drawn here for MscS translate to other channels known to mechano-transduce changes in membrane tension. Indeed, the proposed deformation model would appear explain the mechanosensitivity of PIEZO, which is considerably greater than that of MscS (1.4 mN/m [33] vs ~5 mN/m [8], respectively). In the closed state, PIEZO bends the membrane into a high-curvature dome-like morphology in the 10-nm scale [4]; this large-scale deviation from the conformation that is intrinsically favored by the membrane certainly comes at a great energy cost, which would be made even greater when the membrane is stretched under tension, even minimally. Thus, for PIEZO too would this increased penalty translate into shift in the gating equilibrium, towards the conductive state.

METHODS

MscS expression purification

Full-length wilt-type *E. coli* MscS and the MscS mutant A106V were expressed and purified as previously described [13, 34]. In brief, MscS was sub-cloned into pET28a containing a His6 tag and a thrombin cleavage site on the N-termini. Rosetta 2 (Millipore Sigma). *E. coli* cells were transformed with MscS-pET28a vector and grown overnight in the presences of kanamycin and chloramphenicol. Cells were diluted 1:100 in LB medium and grown at 37°C to an OD600 of 0.8-1.0. Before induction, the cell culture was supplemented to a final concentration of 0.4% glycerol and allowed to cool to 26°C, and protein expression was induced with 0.8mM IPTG. Cells were grown for 4h at 26°C, harvested, and resuspended in PBS pH 7.4 (Sigma), 10% glycerol, protease inhibitors, and homogenized (high-pressure homogenizer, EmulsiFlex-C3). Membranes were isolated via centrifugation at 100,000g for 30 min, and the pellet was resuspended in PBS and 10% glycerol. Solubilization was carried out in DDM (Anatrace) for 4-16h at 4°C, spun down at 100,000g for 30 min, and the supernatant, supplemented with a final concentration of 5mM imidazole (Fisher), was incubated with cobalt resin (Clonetech) for 2-4h at 4 °C. The resin was washed with 20-bed volumes of 1 mM DDM, 10mM imidazole and 10% glycerol in PBS buffer. MscS was eluted in 1 mM DDM, 300mM imidazole, and 10% glycerol in PBS buffer. Final purification was on a Superdex 200 Increase 10/30 column (GE Healthcare) with 1 mM DDM and PBS buffer.

MscS nanodisc preparation

MscS nanodiscs (ND) were prepared following previously described protocol [35] subsequently adapted to use Msp1 E3D1 as scaffold [17]. The molar ratio of MscS:MSP1 E3D1:Lipids was 7:10:650, respectively, after extensive optimizations. Each lipid solution of mixed micelles contained 30-50 mM DDM with a final lipid concentration of 10-17 mM. Mixed micelles contained either (1-palmitoyl-2-oleoyl-sn-glycero-3-phosphocholine) POPC and (1-2-palmitoyl-2-oleoylglycero-3-phosphoglycerol) POPG (4:1) for the reference MscS structure (PC18:1) or (1-2-dimyristoleoyl-sn-glycero-3-phosphocholine) DMPC for the thin bilayer open structure (PC14:1). Additional nanodisc-reconstituted MscS preps were carried out in 1-2-dimyristoyl-sn-glycero-3-phosphocholine or *E coli* polar lipids. Nanodiscs were made by adding mix micelles to protein for 20 minutes on ice. MSP was added to the solution and incubated on ice for 5 minutes. The reconstitution mixture was incubated in activated bio beads (Biorad) overnight at 4°C. The

detergent free mixture was run on a Superdex 200 Increase 10/30 column to separate the empty ND peak. The MscS ND peak was concentrated to ~2mg/ml and stored at 4°C.

EM data collection and structure determination

MscS ND was supplemented with Octyl Maltoside, Fluorinated (Anatrace) to a final concentration of 0.01%. MscS was doubly applied onto Mesh 200 2/1 or Mesh 300 1.2/1.3 Quantifoli holey carbon grids. Grids were flash frozen in a Vitrobot (Thermofisher) set at 3 seconds with a force of 3 with 100% humidity at 22°C. Imaging was carried out on a Titan Krios with a K3 detector in counting mode with a GIF energy filter using Latitude S (Thermofisher). Movies were acquired at 1e-/A2 per frame for 50 frames. Movies were acquired at 1e-/A2 per frame for 50 frames. Motion correction was performed using Motioncor2 [36], and K2 movies were binned by 2. CTF estimation was done using CTFFIND4.1 [37]. Initial particle picking was done using Eman's [38] neural net particle picker or Relion's built-in reference-based auto picker and the coordinates were fed into Relion [39] for particle extraction. Subsequent structure determination steps were done in Relion. An initial 2D refinement was done to remove non-particles and poor-quality classes, which were fed into 3D classification. 3D classification was performed using the MscS nanodisc structure as an initial model. After a subset of particles were identified for the final refinement, the particles underwent per particle CTF refinement followed by Bayesian polishing. Final 3D reconstruction used the classes with both top and side views and refined using a mask that excluded the membrane and his-tag (when necessary) under C7 symmetry. Model building was based on an existing cryo-EM structure of closed-state MscS (PDBID: 6PWN), and used coot to build the remaining TM1, N-terminal domain, and the hook and pore lipids. EM density maps used in subsequent steps were not postprocessed or sharpened. The initially built model was iteratively refined using Coot [40], Chimera [41], MDFF [42] using VMD [43] and NAMD [44] or ChimeraX [45] with the ISOLDE [46] plugin, Arp/Warp [47], and Phenix's [48] real space refine.

Molecular dynamics simulations

All coarse-grained (CG) simulations used the MARTINI 2.2/ElNeDyn22 forcefield [49-51] in GROMACS 2018.8 [52]. The temperature was maintained at 303 K (τ_T = 1 ps) using velocity-rescaling [53], and the pressure was maintained at 1 bar (compressibility = 3×10^{-4} bar^{-1}) with the Berendsen method [54] during equilibration, then with the Parrinello-Rahman semi-isotropic barostat [55] during data production. An 11-Å cutoff was used for both reaction-field electrostatics and van der Waals interactions.

The CG protein-membrane systems were constructed by introducing coarse-grained protein structures into pre-equilibrated lipid bilayers of various compositions and sizes. A POPC membrane was used because previous functional studies have shown that MscS behaves similarly in PC and PE/PC (7:3) membranes [26]. A 4:1 POPC:POPG membrane was also included because the structure of closed MscS was purified in a nanodisc with that composition [17]. For the DMPC simulations, we adapted the DLPC lipid type in MARTINI as in this representation it features the same chain-length. All systems included a 150 mM NaCl solution plus counterions to neutralize the total bilayer charge. These bilayers we initially constructed using the *insane* protocol [51], then energy-minimized with the steepest-descent energy algorithm (500,000 steps) and then equilibrated in three stages (1 ns, 2-fs timestep, τ_P = 1 ps; 1 ns, 10 fs timestep, τ_P = 2 ps; 1 ns, 20 fs timestep, τ_P = 4 ps). Production simulations were then carried out with 20-fs timesteps for 2-10 μs depending on the system (τ_P = 12 ps). The resulting trajectories were extensively analyzed (bilayer thickness, area per lipid, second-rank order parameter, lipid length, lipid splay, interdigitation, interleafleat contacts) using MOSAICS [56] to ascertain the simulations reproduce the expected morphology. The last snapshot in each case was used to construct the protein-membrane systems.

All simulations of MscS and MSL1 are based on experimental structures, including that reported in this study. Previously reported structures are: wild-type MscS, PDB entry 6PWP, resolution 4.1 Å [17]; MscS mutant D67R1, 5AJI, 3.0 Å [14]; MscS mutant A106V, 2VV5, 3.5 Å [13]; MSL1 mutant I234A/A235I, 6LYP, 3.3 Å [19]; MSL1 mutant A320V, 6VXN, 3.0 Å [18]. In all cases, the atomic structures were coarse-grained using a modified version of *martinize.py* [57] that allows for customization of neutral N- and C-termini and protonation states of aspartate and glutamate. The simulations used only the constructs and fragments resolved experimentally, with no additional modeling except for the reversal of all mutations, and the addition of water to fill the central pores. To construct the protein-membrane simulation systems, the CG protein structures (with pores filled) were superposed onto the equilibrated CG bilayers, aligning the centers of the transmembrane domains (residues 21-44 and 80-89 for MscS; 204-323 for MSL1) with those of the lipid the bilayers, then removing overlapping lipids and solvent. Additional counterions were added to neutralize the net charge of the protein. The resulting molecular systems were then energy-minimized (2000 steepest-descent steps) and equilibrated in four stages (0.01 ns, 2-fs timestep, τ_P = 5 ps; 1 ns, 2-fs timestep, τ_P = 1 ps; 1 ns, 10-fs timestep, τ_P = 2 ps; 1 ns, 20-fs

timestep, τ_P = 4 ps). Data production simulations followed, using a 20-fs timestep (τ_P = 12 ps) for a total of 20-80 μs, depending on the system. It is worth nothing that the protein elastic networks used in these simulations differ from those produced by default with *martinize*; force constants and cut-off distances were optimized for each channel to minimize changes relative to the experimental structure. Specifically, RMS deviations in the core transmembrane domain (residues 21-44 and 80-89 for MscS; 204-323 for MSL1) are limited to 1 Å, and those of the protein overall are limited to 1.5 Å. For MscS, these limits imply elastic bonds defined using lower and upper cut-off distances of 5 and 11 Å, respectively, and a force constant of 500 kJ/mol. For MSL1, the force constant was 750 kJ/mol, and the lower and upper cut-off distances were 5 and 14 Å for the transmembrane domain and 5 and 9 Å elsewhere.

All-atom (AA) simulation systems for closed MscS in POPC and DMPC bilayers were constructed on the basis of representative snapshots of the corresponding CG trajectories. To select these snapshots among all obtained, a scoring system was devised that considers (1) the instantaneous RMS deviation of the protein backbone relative to the experimental structure and (2) the degree of similarity between the instantaneous shapes of the bilayer and the time-average of that shape. The snapshots selected are those that minimize the former while maximizing the latter. To construct the AA systems, protein, membrane and solvent were initially "backmapped" using a modified version of *backward.py* [58]. In both systems, however, the backmapped protein structure was replaced with the experimental atomic structure (PDB 6PWP), after alignment of their Cα traces. The protein construct studied includes residues 16-278 of each chain. This atomic structure had been previously processed to add structural water, using Dowser [59], as well as hydrogens, using CHARMM [60]. The resulting systems were further minimized and equilibrated in NAMD [44], using the CHARMM36 forcefield [61, 62]. Minimization consisted of two stages of 5000 steps each: the first had constraints on water hydrogens and positional harmonic restraints on the protein's heavy atoms and dowser waters. The second was 5000 steps with dihedral restraints on the χ_1, ψ, and φ angles of the protein with force constant 256 kJ/mol and bond constraints on all hydrogen bonds; all restraints were harmonic. The equilibration consisted of six stages, all using 2-fs timesteps: 1) φ/ψ force constant 256 kJ/mol, χ_1 force constant 256 kJ/mol, 2) φ/ψ 256 kJ/mol, χ_1 64 kJ/mol, 3) φ/ψ 64 kJ/mol, χ_1 16 kJ/mol, 4) φ/ψ 16 kJ/mol, χ_1 4 kJ/mol, 5) φ/ψ 4 kJ/mol, χ_1 1 kJ/mol, and 6) φ/ψ 4 kJ/mol, no χ_1 restraint. The pressure was maintained at 1.01325 bar (oscillation time scale = 200 fs; damping time scale = 50 fs) with using the Nosé-Hoover

Langevin piston pressure control. A cut-off distance of 12 Å with switching function starting at 10 Å was used for van der Waals interactions. The particle-mesh Ewald method was used for long-range electrostatic forces. For non-bonded interactions, the pairs list distance was 14 Å. The POPC system was simulated at 298 K and the DMPC system was simulated at 303 K to avoid a phase transition [63] using Langevin dynamics ($\lambda = 1$ ps^{-1}).

Production trajectories for both the POPC and DMPC systems, each 10-μs long, were calculated with an ANTON2 supercomputer [64], using the CHARMM36 forcefield. The trajectories were calculated using the Multigrator integrator [65], the Nosé-Hoover thermostat (298 K for POPC, 308 K for DMPC; $\tau_T = 0.047$ ps for both) and the semi-isotropic MTK barostat (pressure 1.0, $\tau_P = 0.047$ ps) [66]. To preclude major changes in the protein backbone, these simulations implemented a set of weak non-harmonic ψ and φ dihedrals restraints, as described previously [67]. A single set of target dihedral angles was used across the heptamer, calculated by averaging ψ and φ angles across chains; the force constant was 4 kJ/mol. CG and AA trajectories were analyzed with MOSAICS [56], VMD [43] and MDAnalysis [68].

ACKNOWLEDGEMENTS

This study was funded by the Intramural Research Program of the National Institutes of Health (NIH) (Y.C.P and J.D.F.G) as well as by NIH grant R01GM131191 (B.R. and E.P). Computational resources were provided by the NIH High-Performance Computing System Biowulf and by the Pittsburgh Supercomputing Center, which provided access to an Anton2 computer donated by D.E. Shaw Research and supported through NIH grant R01GM116961. The authors thank Dr. Wenchang Zhou for his contributions at the onset of this study and Dr. Nathan Bernhardt for his assistance with data analysis.

DATA AVAILABILITY

EM maps and atomic models have been deposited in the Electron Microscopy Data Bank (accession number EMD-27337) and the Protein Data Back (entry code 8DDJ).

REFERENCES

1. Zhang W, Cheng LE, Kittelmann M, Li J, Petkovic M, Cheng T, Jin P, Guo Z*, et al.* Ankyrin repeats convey force to gate the NOMPC mechanotransduction channel. *Cell*, **2015**, 162:1391-1403.
2. Katta S, Krieg M, and Goodman MB. Feeling force: physical and physiological principles enabling sensory mechanotransduction. *Annu Rev Cell Dev Biol*, **2015**, 31:347-371.
3. Cox CD, Bavi N, and Martinac B. Bacterial mechanosensors. *Annu Rev Physiol*, **2018**, 80:71-93.
4. Guo YR and MacKinnon R. Structure-based membrane dome mechanism for Piezo mechanosensitivity. *eLife*, **2017**, 6.
5. Kung C. A possible unifying principle for mechanosensation. *Nature*, **2005**, 436:647-654.
6. Anishkin A, Loukin SH, Teng J, and Kung C. Feeling the hidden mechanical forces in lipid bilayer is an original sense. *Proc Natl Acad Sci USA*, **2014**, 111:7898-7905.
7. Kung C, Martinac B, and Sukharev S. Mechanosensitive channels in microbes. *Annu Rev Microbiol*, **2010**, 64:313-329.
8. Haswell ES, Phillips R, and Rees DC. Mechanosensitive channels: what can they do and how do they do it? *Structure*, **2011**, 19:1356-1369.
9. Wilson ME, Maksaev G, and Haswell ES. MscS-like mechanosensitive channels in plants and microbes. *Biochemistry*, **2013**, 52:5708-5722.
10. Flegler VJ, Rasmussen A, Rao S, Wu N, Zenobi R, Sansom MSP, Hedrich R, Rasmussen T*, et al.* The MscS-like channel YnaI has a gating mechanism based on flexible pore helices. *Proc Natl Acad Sci USA*, **2020**, 117:28754-28762.

11. Pivetti CD, Yen MR, Miller S, Busch W, Tseng YH, Booth IR, and Saier MH, Jr. Two families of mechanosensitive channel proteins. *Microbiol Mol Biol Rev*, **2003**, 67:66-85.

12. Bass RB, Strop P, Barclay M, and Rees DC. Crystal structure of *Escherichia coli* MscS, a voltage-modulated and mechanosensitive channel. *Science*, **2002**, 298:1582-1587.

13. Wang W, Black SS, Edwards MD, Miller S, Morrison EL, Bartlett W, Dong C, Naismith JH, *et al.* The structure of an open form of an *E. coli* mechanosensitive channel at 3.45 A resolution. *Science*, **2008**, 321:1179-1183.

14. Pliotas C, Dahl AC, Rasmussen T, Mahendran KR, Smith TK, Marius P, Gault J, Banda T, *et al.* The role of lipids in mechanosensation. *Nat Struct Mol Biol*, **2015**, 22:991-998.

15. Flegler VJ, Rasmussen A, Borbil K, Boten L, Chen HA, Deinlein H, Halang J, Hellmanzik K, *et al.* Mechanosensitive channel gating by delipidation. *Proc Natl Acad Sci USA*, **2021**, 118.

16. Zhang Y, Daday C, Gu RX, Cox CD, Martinac B, de Groot BL, and Walz T. Visualization of the mechanosensitive ion channel MscS under membrane tension. *Nature*, **2021**, 590:509-514.

17. Reddy B, Bavi N, Lu A, Park Y, and Perozo E. Molecular basis of force-from-lipids gating in the mechanosensitive channel MscS. *eLife*, **2019**, 8.

18. Deng Z, Maksaev G, Schlegel AM, Zhang J, Rau M, Fitzpatrick JAJ, Haswell ES, and Yuan P. Structural mechanism for gating of a eukaryotic mechanosensitive channel of small conductance. *Nat Commun*, **2020**, 11:3690.

19. Li Y, Hu Y, Wang J, Liu X, Zhang W, and Sun L. Structural insights into a plant mechanosensitive ion channel MSL1. *Cell Rep*, **2020**, 30:4518-4527 e4513.

20. Marrink SJ and Mark AE. Effect of undulations on surface tension in simulated bilayers. *J Phys Chem B*, **2001**, 105:6122-6127.

21. Pravda L, Sehnal D, Tousek D, Navratilova V, Bazgier V, Berka K, Svobodova Varekova R, Koca J, *et al.* MOLEonline: a web-based tool for analyzing channels, tunnels and pores. *Nucleic Acids Res*, **2018**, 46:W368-W373.

22. Miyazaki C, Kuroda M, Ohta A, and Shibuya I. Genetic manipulation of membrane phospholipid composition in *Escherichia coli*: pgsA mutants defective in phosphatidylglycerol synthesis. *Proc Natl Acad Sci USA*, **1985**, 82:7530-7534.

23. Schenkel LC and Bakovic M. Formation and regulation of mitochondrial membranes. *Int J Cell Biol*, **2014**, 2014:709828.

24. Corradi V, Mendez-Villuendas E, Ingolfsson HI, Gu RX, Siuda I, Melo MN, Moussatova A, DeGagne LJ, *et al.* Lipid-protein interactions are unique fingerprints for membrane proteins. *ACS Cent Sci*, **2018**, 4:709-717.

25. Edwards MD, Li Y, Kim S, Miller S, Bartlett W, Black S, Dennison S, Iscla I, *et al.* Pivotal role of the glycine-rich TM3 helix in gating the MscS mechanosensitive channel. *Nat Struct Mol Biol*, **2005**, 12:113-119.

26. Nomura T, Cranfield CG, Deplazes E, Owen DM, Macmillan A, Battle AR, Constantine M, Sokabe M, *et al.* Differential effects of lipids and lyso-lipids on the mechanosensitivity of the mechanosensitive channels MscL and MscS. *Proc Natl Acad Sci USA*, **2012**, 109:8770-8775.

27. Rasmussen T, Rasmussen A, Singh S, Galbiati H, Edwards MD, Miller S, and Booth IR. Properties of the mechanosensitive channel MscS pore revealed by tryptophan scanning mutagenesis. *Biochemistry*, **2015**, 54:4519-4530.

28. Malcolm HR, Blount P, and Maurer JA. The mechanosensitive channel of small conductance (MscS) functions as a Jack-in-the box. *Biochim Biophys Acta*, **2015**, 1848:159-166.

29. Gullingsrud J and Schulten K. Lipid bilayer pressure profiles and mechanosensitive channel gating. *Biophys J*, **2004**, 86:3496-3509.

30. Bavi N, Cortes DM, Cox CD, Rohde PR, Liu W, Deitmer JW, Bavi O, Strop P, *et al.* The role of MscL amphipathic N terminus indicates a blueprint for bilayer-mediated gating of mechanosensitive channels. *Nat Commun*, **2016**, 7:11984.

31. Zhou W, Fiorin G, Anselmi C, Karimi-Varzaneh HA, Poblete H, Forrest LR, and Faraldo-Gomez JD. Large-scale state-dependent membrane remodeling by a transporter protein. *eLife*, **2019**, 8.

32. Fiorin G, Marinelli F, and Faraldo-Gomez JD. Direct derivation of free energies of membrane deformation and other solvent density variations from enhanced sampling molecular dynamics. *J Comput Chem*, **2020**, 41:449-459.

33. Lewis AH and Grandl J. Mechanical sensitivity of Piezo1 ion channels can be tuned by cellular membrane tension. *eLife*, **2015**, 4.

34. Vasquez V, Cortes DM, Furukawa H, and Perozo E. An optimized purification and reconstitution method for the MscS channel: strategies for spectroscopical analysis. *Biochemistry*, **2007**, 46:6766-6773.

35. Ritchie TK, Grinkova YV, Bayburt TH, Denisov IG, Zolnerciks JK, Atkins WM, and Sligar SG. Reconstitution of membrane proteins in phospholipid bilayer nanodiscs. *Methods Enzymol*, **2009**, 464:211-231.

36. Zheng SQ, Palovcak E, Armache JP, Verba KA, Cheng Y, and Agard DA. MotionCor2: anisotropic correction of beam-induced motion for improved cryo-electron microscopy. *Nat Methods*, **2017**, 14:331-332.

37. Rohou A and Grigorieff N. CTFFIND4: fast and accurate defocus estimation from electron micrographs. *J Struct Biol*, **2015**, 192:216-221.

38. Tang G, Peng L, Baldwin PR, Mann DS, Jiang W, Rees I, and Ludtke SJ. EMAN2: an extensible image processing suite for electron microscopy. *J Struct Biol*, **2007**, 157:38-46.

39. Scheres SH. RELION: implementation of a Bayesian approach to cryo-EM structure determination. *J Struct Biol*, **2012**, 180:519-530.

40. Emsley P, Lohkamp B, Scott WG, and Cowtan K. Features and development of COOT. *Acta Crystallogr D Biol Crystallogr*, **2010**, 66:486-501.

41. Pettersen EF, Goddard TD, Huang CC, Couch GS, Greenblatt DM, Meng EC, and Ferrin TE. UCSF Chimera: a visualization system for exploratory research and analysis. *J Comput Chem*, **2004**, 25:1605-1612.

42. McGreevy R, Singharoy A, Li Q, Zhang J, Xu D, Perozo E, and Schulten K. xMDFF: molecular dynamics flexible fitting of low-resolution X-ray structures. *Acta Crystallogr D Biol Crystallogr*, **2014**, 70:2344-2355.

43. Humphrey W, Dalke A, and Schulten K. VMD: visual molecular dynamics. *J Mol Graph*, **1996**, 14:33-38, 27-38.

44. Phillips JC, Hardy DJ, Maia JDC, Stone JE, Ribeiro JV, Bernardi RC, Buch R, Fiorin G, *et al.* Scalable molecular dynamics on CPU and GPU architectures with NAMD. *J Chem Phys*, **2020**, 153:044130.

45. Goddard TD, Huang CC, Meng EC, Pettersen EF, Couch GS, Morris JH, and Ferrin TE. UCSF ChimeraX: meeting modern challenges in visualization and analysis. *Protein Sci*, **2018**, 27:14-25.

46. Croll TI. ISOLDE: a physically realistic environment for model building into low-resolution electron-density maps. *Acta Crystallogr D Struct Biol*, **2018**, 74:519-530.

47. Langer G, Cohen SX, Lamzin VS, and Perrakis A. Automated macromolecular model building for X-ray crystallography using ARP/wARP version 7. *Nat Protoc*, **2008**, 3:1171-1179.

48. Adams PD, Afonine PV, Bunkoczi G, Chen VB, Davis IW, Echols N, Headd JJ, Hung LW, *et al.* PHENIX: a comprehensive Python-based system for macromolecular structure solution. *Acta Crystallogr D Biol Crystallogr*, **2010**, 66:213-221.

49. Marrink SJ, de Vries AH, and Mark AE. Coarse grained model for semiquantitative lipid simulations. *J Phys Chem B*, **2004**, 108:750-760.

50. Marrink SJ, Risselada HJ, Yefimov S, Tieleman DP, and de Vries AH. The MARTINI force field: coarse grained model for biomolecular simulations. *J Phys Chem B*, **2007**, 111:7812-7824.

51. Wassenaar TA, Ingolfsson HI, Bockmann RA, Tieleman DP, and Marrink SJ. Computational lipidomics with *insane*: a versatile tool for generating custom membranes for molecular simulations. *J Chem Theory Comput*, **2015**, 11:2144-2155.

52. Abraham MJ, Murtola T, Schulz R, Pall S, Smith JC, Hess B, and Lindahl E. GROMACS: high performance molecular simulations through multi-level parallelism from laptops to supercomputers. *SoftwareX*, **2015**, 1-2:19-25.

53. Bussi G, Donadio D, and Marrinello M. Canonical sampling through velocity rescaling. *J Chem Phys*, **2007**, 126.

54. Berendsen HJC, Postma JPM, van Gunsteren WF, DiNola A, and Haak JR. Molecular dynamics with coupling to an external bath. *J Chem Phys*, **1984**, 81.

55. Parrinello M and Rahman A. Polymorphic transitions in single crystals: A new molacular dynamics method. *J Appl Phys*, **1981**, 52:7182-7190.

56. Bernhardt N and Faraldo-Gomez JD. MOSAICS: a software suite for spatially resolved analyses of lipid bilayer structure and dynamics in simulated trajectories of membrane systems. *Under Review*, **2022**.

57. de Jong DH, Singh G, Bennett WF, Arnarez C, Wassenaar TA, Schafer LV, Periole X, Tieleman DP, *et al.* Improved parameters for the Martini coarse-grained protein force field. *J Chem Theory Comput*, **2013**, 9:687-697.

58. Wassenaar TA, Pluhackova K, Bockmann RA, Marrink SJ, and Tieleman DP. Going backward: a flexible geometric approach to reverse transformation from coarse grained to atomistic models. *J Chem Theory Comput*, **2014**, 10:676-690.

59. Zhang L and Hermans J. Hydrophilicity of cavities in proteins. *Proteins*, **1996**, 24:433-438.

60. Brooks BR, Brooks CL, Mackerell AD, Nilsson L, Petrella RJ, Roux B, Won Y, Archontis G, *et al.* CHARMM: the biomolecular simulation program. *J Comput Chem*, **2009**, 30:1545-1614.

61. Klauda JB, Venable RM, Freites JA, O'Connor JW, Tobias DJ, Mondragon-Ramirez C, Vorobyov I, MacKerell AD, Jr., *et al.* Update of the CHARMM all-atom additive force field for lipids: validation on six lipid types. *J Phys Chem B*, **2010**, 114:7830-7843.

62. Best RB, Zhu X, Shim J, Lopes PE, Mittal J, Feig M, and Mackerell AD, Jr. Optimization of the additive CHARMM all-atom protein force field targeting improved sampling of the backbone phi, psi and side-chain chi_1 and chi_2 dihedral angles. *J Chem Theory Comput*, **2012**, 8:3257-3273.

63. Khakbaz P and Klauda JB. Investigation of phase transitions of saturated phosphocholine lipid bilayers via molecular dynamics simulations. *Biochim Biophys Acta Biomembr*, **2018**, 1860:1489-1501.

64. Shaw DE, Grossman JP, Ban JA, Batson B, Butts JA, Chao JC, Deneroff MM, Dror RO*, et al.* Anton 2: raising the bar for performance and programmability in a special-purpose molecular dynamics supercomputer. *IEEE,* **2014**, 41–53.

65. Lippert RA, Predescu C, Ierardi DJ, Mackenzie KM, Eastwood MP, Dror RO, and Shaw DE. Accurate and efficient integration for molecular dynamics simulations at constant temperature and pressure. *J Chem Phys*, **2013**, 139.

66. Martyna G, Tobias D, and Klein M. Constant pressure molecular dynamics algorithms. *J Chem Phys*, **1994**, 101.

67. Tan XF, Bae C, Stix R, Fernandez-Marino AI, Huffer K, Chang TH, Jiang J, Faraldo-Gomez JD*, et al.* Structure of the *Shaker* K_v channel and mechanism of slow C-type inactivation. *Sci Adv*, **2022**, 8:eabm7814.

68. Michaud-Agrawal N, Denning EJ, Woolf TB, and Beckstein O. MDAnalysis: a toolkit for the analysis of molecular dynamics simulations. *J Comput Chem*, **2011**, 32:2319-2327.